JOM, Vol. 75, No. 3, 2023
https://doi.org/10.1007/s11837-022-05619-z

Lanthanum-Promoted Nickel-Based Catalysts for the Dry Reforming of Methane at Low Temperatures

ZOULIKHA ABDELSADEK ,[1,2,6] HASAN KÖTEN ,[3] SERGIO GONZALEZ-CORTES ,[4] OUIZA CHERIFI,[2] DJAMILA HALLICHE ,[2] and PATRICK J. MASSET [5,7]

1.—Institute of Electrical and Electronics Engineering, University of M'hamed-Bougara, Independence Avenue, 35000 Boumerdès, Algeria. 2.—Laboratory of Chemistry and Natural Gas, Faculty of Chemistry, USTHB, B.P. 32 El-Alia, 16111 Bab-Ezzouar, Algeria. 3.—Mechanical Engineering Department, Istanbul Medeniyet University, 34700 Uskudar, Istanbul, Turkey. 4.—Inorganic Chemistry Laboratory, Department of Chemistry, University of Oxford, South Parks Road, Oxford OX1 3QR, UK. 5.—Faculty of Materials Science and Engineering, Warsaw University of Technology, Woloska 141, 02-507 Warsaw, Poland. 6.—e-mail: z.abdelsadek@univ-boumerdes.dz. 7.—e-mail: patrick.masset@pw.edu.pl

In recent decades, considerable attention has been paid to the catalytic dry reforming of methane to obtain syngas. This reaction has very important environmental implications due to the utilization of CH_4 and CO_2, gases that contribute to the greenhouse effect. The dry reforming of methane is normally carried out over strong basic catalysts with noble metals. Nickel has emerged as an interesting alternative, although it tends to deactivate and form carbon whiskers, which could block the reactor. It is therefore necessary to improve their catalytic performance (conversion, selectivity and stability). In this work, $Ni_{0.69}La_{0.31}$ and $Ni_{0.14}Mg_{0.55}La_{0.31}$ were studied in the dry methane reforming reaction. The precursors were prepared by co-precipitation and the oxide phases were obtained by calcining these precursors at 450°C/6 h. The XRD diagrams of the calcined samples show the formation of mixed oxide phases with a periclase-like structure. Analysis of the temperature-programmed reduction shows that the presence of Mg shifts the reduction to higher temperatures. The catalysts, reduced at 650°C, were tested in this reaction as a function of operating time at 650°C. No deactivation occurred after 20 h of operation. Furthermore, the combination of Mg and La drastically improves the conversion and selectivity of the catalyst (> 95%).

INTRODUCTION

Reforming of methane with carbon dioxide, also referred as dry reforming of methane (DRM reaction) (Eq. 1), is one of the routes to produce syngas (H_2 and CO mixture). It represents an industrially relevant process and was revealed adequate to produce H_2/CO equimolar ratio syngas, especially interesting for the Fisher-Tropsh synthesis.[1]

$$CH_4 + CO_2 \rightleftarrows 2H_2 + 2CO \quad (1)$$

(Received August 4, 2022; accepted November 21, 2022; published online December 19, 2022)

In addition, the DRM reaction meets the criteria of green chemistry and environmental protection as it converts greenhouse gases (i.e., CH_4 and CO_2) into valuable feedstocks or intermediate products for the industry. The dry reforming of methane needs strong basic catalysts. Great efforts have been focused on the development of catalysts which show high activity and stability. Supported metal catalysts have been used in the reforming reaction of hydrocarbons and are conventionally prepared by impregnation of different supports. This method is not fully reproducible and may give rise to some inhomogeneity in the distribution of the metal of the surface. Moreover, the fine metal particles obtained tend to sinter at high temperature, resulting in catalyst deactivation. It is recognized that most of

the group VIII metals are effective for CH_4/CO_2 reaction in terms of conversion (CH_4 and CO_2) and selectivity to synthesis gas. Noble metals such as Ru, Rh, Pt and Ir… have successfully been employed as highly active catalysts for CO_2 reforming of CH_4.[1,2] However, the high cost and limited availability of noble metals have stimulated researching for cheaper metals such as Ni and Co. Recently special attention has been paid to a method of preparation called "solid phase crystallization". This method basically consists in obtaining a crystalline phase where metal ions such as Ni^{2+} and Co^{2+} are in well-defined positions of the structure, which on further calcination and reduction may result in the formation of highly dispersed metal particles onto an oxidic support.[3]

The hydrotalcite structure can be considered positively charged brucite-type octahedral sheets in which a part of the Mg^{2+} is substituted by a trivalent metal like Al^{3+} generating a partial positive charge that is compensated with carbonate anions and water molecules located in the interlayer space (Fig. 1).

The corresponding chemical formula is: $[M_{1-x}{}^{2+} M_x{}^{3+} (OH)_2]^{x+}[A^{n-}]_{x/n}.m\ H_2O$, where and M^{2+} and M^{3+} are di- and trivalent metals, respectively. Nevertheless, it is possible to prepare different hydrotalcites by the partial or total substitution of Mg^{2+} and Al^{3+} with other divalent (Ni^{2+}, Co^{2+}, Cu^{2+} …) or trivalent cations (Ce^{3+}, Y^{3+}…). Hydrotalcites retain their layered structure up to 400°C and even at higher temperatures for large-area mixed metal oxides. Calcination of hydrotalcite leads to the formation of mixed-oxide phases that are potentially useful as catalysts or catalyst precursors owing to their following properties[4–7]: (1) simple preparation method that is easy to perform in the laboratory and for industrial upscaling; (2) thermostable phases with a specific surface which varies between 100 and 300 m^2/g; (3) adjustable Brönsted acid/base properties; (4) good dispersion of the active phase. Hydrotalcite (HT) as catalyst is also widely investigated in CO_2 methane reforming[8] (Fig. 2).

Three main ways are used to obtain supported metal catalysts derived from hydrotalcite[4] (Fig. 3). The first is the synthesis of hydrotalcite as precursor with desired metal cations located in the brucite-like layers. The second is by an anionic exchange from an initial and already prepared HDL matrix. The third method is based on calcination of inorganic or organometallic precursors of metal hydrotalcite material after the reconstruction of hydrotalcite matrix. To obtain the final supported metal catalysts, all methods of preparation involve calcination and then reduction as activation steps.

Ni-based catalysts are the most popular catalysts; they have been considered a cheaper alternative to noble metals in dry reforming of methane given that Ni is present similar TOFs. The major problem of Ni catalysts is their deactivation by the sintering of Ni active phase and/or carbon deposition, which blocks the catalyst pores and acts as an encapsulation of the active sites. The most recent studies focus on the investigation of metal support interactions and/or use of promoters to improve the activity, selectivity and stability of Ni-based catalysts. The modification of acid-basic and redox properties of the catalysts testing different promoters permits the inhibition of carbon deposition.[6,9]

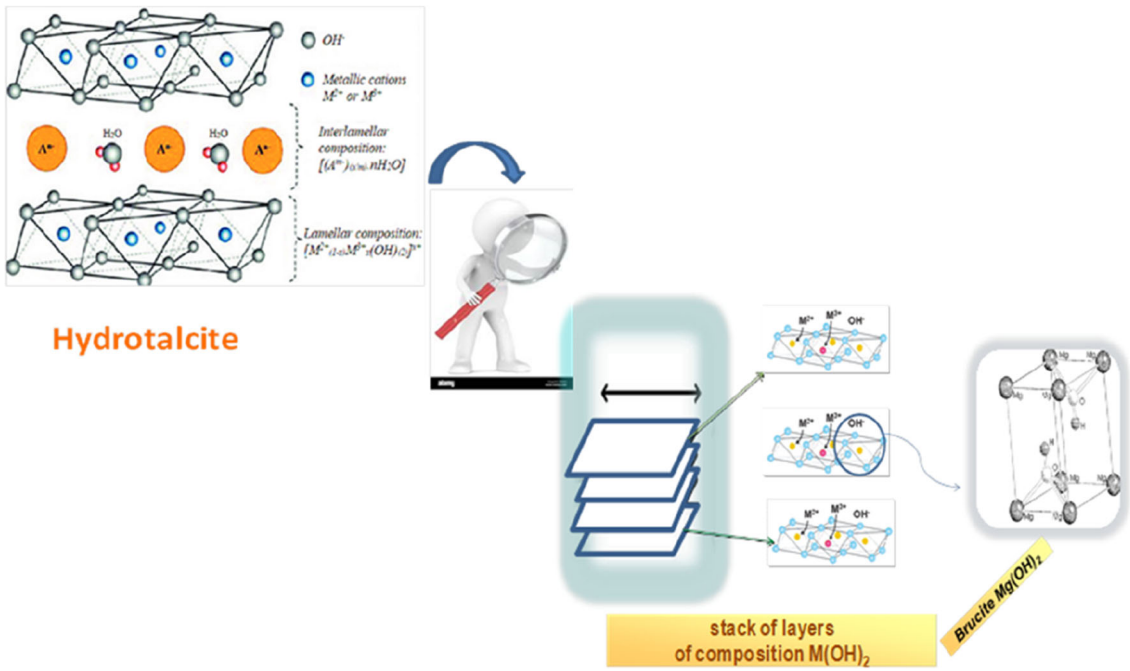

Fig. 1. Synthesis route to obtain the hydrotalcite structure.

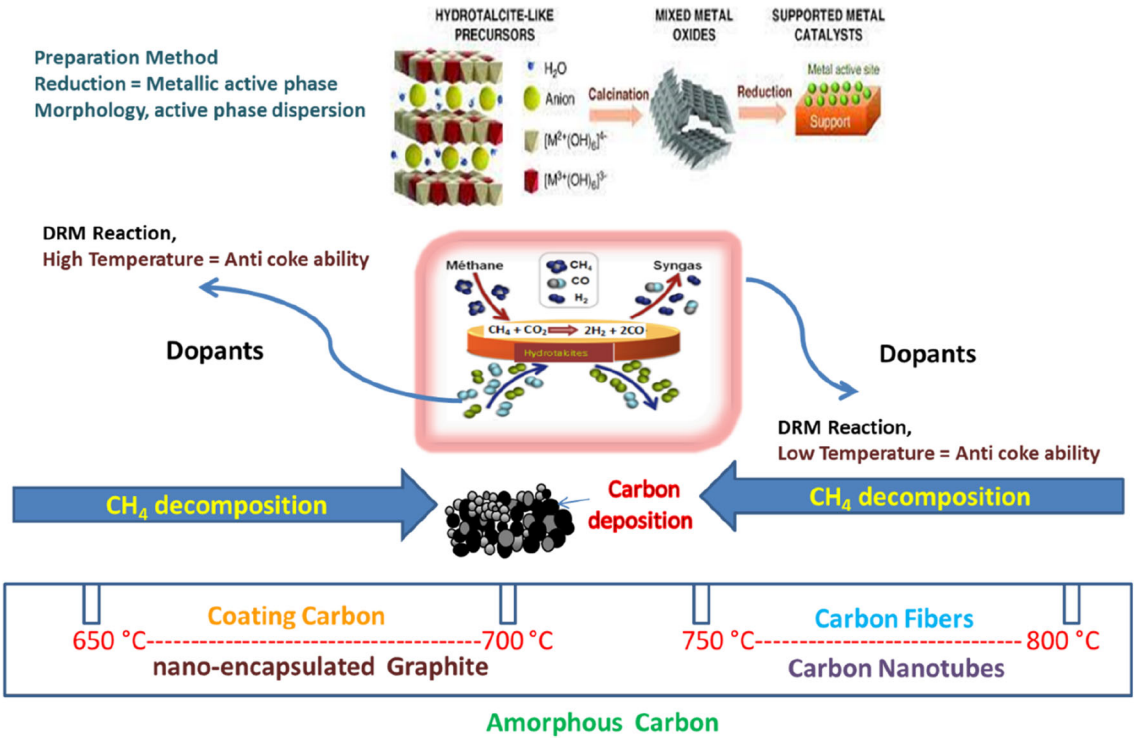

Fig. 2. The application of hydrotalcite in dry reforming of methane.

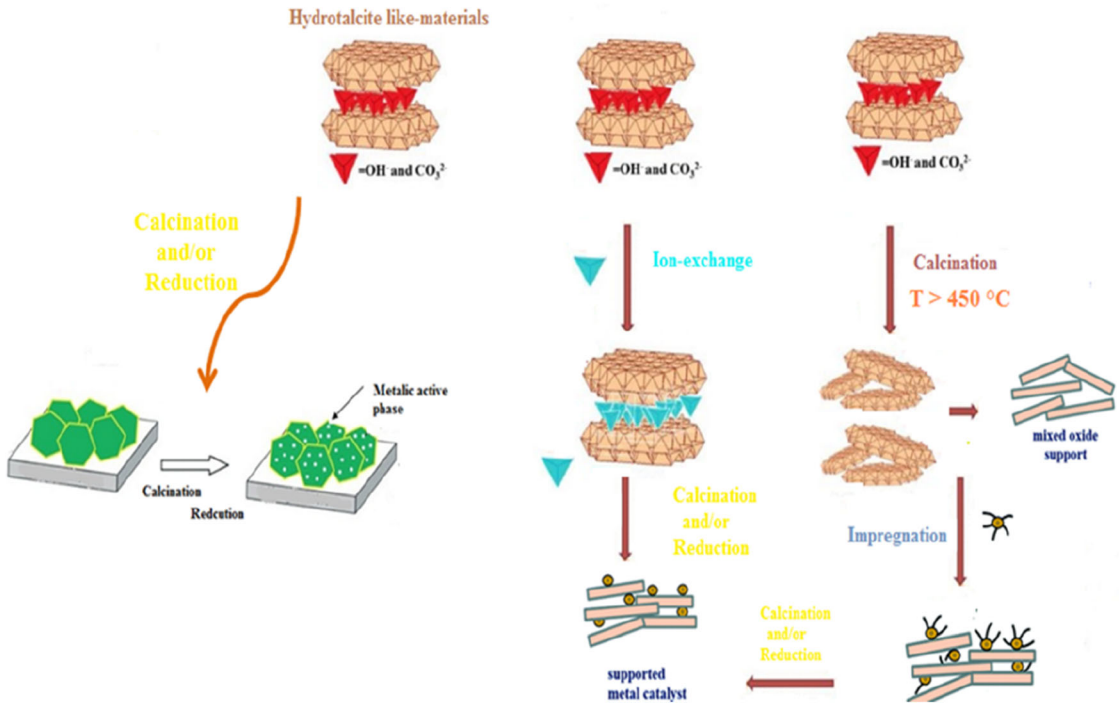

Fig. 3. Different routes used to prepare supported metal catalysts from hydrotalcite.

Lanthanides are considered great and sustainable basic promoters (La_2O_3) as they can reinforce a great adsorption of CO_2 on support which hinders the formation of carbon deposits via reverse disproportionation.[9] Furthermore, it has been reported that the La_2O_3 phase can be converted into $La_2O_2CO_3$ at 600°C ($La_2O_3 + CO_2 \rightarrow La_2O_2CO_3$). It has been proved that the coke deposits on the interface between Ni and $La_2O_2CO_3$ can be gasified through the following reaction: $La_2O_2CO_3 + C \rightarrow$

La_2O_3 + 2CO.[9] Simultaneously, this reaction hinders the formation of carbon deposition on catalytic surface and produces CO as part of the syngas.

Verykios et al.[10] carried out a comparative study of two supported catalysts prepared by incorporation of Ni onto lanthanum oxide La_2O_3 (Ni/La_2O_3) support and Ni over aluminium oxide Al_2O_3 (Ni/Al_2O_3). They concluded that La_2O_3 might be presented as dynamic oxygen supplier and was enhancing the catalytic performances because of the formation of oxy-carbonate phase ($La_2O_2CO_3$), which is responsible for the gasifying of the carbon deposits and provides higher catalyst stability. In addition, it impedes the sintering of the active metallic phase metal leading to an enhanced dispersion of the Ni metal that reduces the coke deposition. The high dispersion of Ni species restrains the rate of carbon deposition, which enhances the stability of the catalyst.[9,11]

Xiaopeng et al.[9] reported that the presence of lanthanum evidently improved the reforming catalytic activity in 600–700°C temperature range. The doping of La in the NiMgAl matrix increased the total amount of basic sites and surface Ni content. It led to the formation of a narrower Ni metal particle size distribution between 5 and 11 nm. In addition, lanthanum significantly improved the stability of the NiMgAl catalysts by suppressing the coke deposition. The effective inhibition of cooking by lanthanum is due to the increase of basicity of the catalysts with the formation of $La_2O_2CO_3$ phase, which improves the dispersion of nickel metal.

Lanthanum doping in Ni-based catalysts shows high resistance to carbon deposition with good catalytic performances and stability. Hydrotalcite-derived Ni-based catalysts exhibit a high dispersion of the active phase Ni^0 particles that develop the catalytic performances for dry methane reforming.[9] Lanthanum-Ni-based catalysts derived from hydrotalcite can exhibit a significant catalytic activity for CO_2 methane reforming. According to the literature and to the best of our knowledge, there are no details on the effect of lanthanum in the structure and its influence and mechanism on the catalytic performances of hydrotalcite-derived Ni catalysts for dry methane reforming.[9]

Academic research has largely focused on increasing the dispersion of the active phase, especially for dry methane reforming. A support with a high specific surface allows a good dispersion of the metallic active phase. Thus, the confinement of the metal particles provided by the support not only leads to a high dispersion of the active metals, but it also exerts a spatial restriction on the metal particles preventing their sintering.[12] The confinement or integration of metal or metal oxide nanoparticles (NPs) in a closed structure (cavities or channels) such as a core–shell, core–shell, mesopore or even lamellar structure leads to essentially better catalytic performance compared to conventional supported catalysts.[11] However, the controllable preparation of core–shell catalytic systems is difficult.

The objective of this work is to demonstrate the interest of La-promoted nickel-based catalysts for the dry reforming of CO_2 at low reaction temperature, i.e., 650°C. Based on the results obtained with MgAl-hydrotalcite matrices,[6] the two catalysts NiLa-DHc-R and NiMgLa-DHc-R were selected, and it was proposed to substitute totally Al by La and Mg by Ni to show the influence of Mg on the catalytic performances (CH_4 and CO_2 conversion, stability and deactivation). The purpose of the present work was to prepare and study fine-dispersed lamellar hydrotalcite-like compounds with La (and Mg) using a reproducible method (continuous co-precipitation). A comparative study of the structural and textural properties with the catalytic performance of $Ni_{0.69}La_{0.31}$ and $Ni_{0.14}Mg_{0.55}La_{0.31}$ was carried out to gain insight into the lanthanum effect over the Ni-based catalyst in the DRM reaction.

EXPERIMENTAL

Materials Preparation

The derived hydrotalcite samples were prepared by the continuous co-precipitation method reported by Miyata et al.[4] (Fig. 4) from two aqueous solutions: (1) metal nitrate ($Ni^{2+}$and or Mg^{2+}, Al^{3+} or La^{3+} cations)-containing solution and (2) alkaline solution with sodium carbonate as precipitant and sodium hydroxide to monitor the pH. Co-precipitation was carried out with constant stirring at 70°C keeping the pH constant (11 ± 0.1) by adjusting the flow rate of the NaOH (1 M) solution. The material was cooled to room temperature, filtered and washed with a large amount of deionized water to pH 7 for complete removal of Na^+ and dried at 80°C for 15 h. The precursors obtained were calcined at 450°C for 6 h (4°C/min). The low value calcination temperature, i.e., 450°C, was used to study the oxide catalyst-derived hydrotalcites. The solids obtained were labelled as follows:

- Non-calcined samples: NiLa-DH, NiMgLa-DH, (DH: derived hydrotalcite).
- Calcined samples: NiLa-DHc, NiMgLa-DHc, (DHc: derived hydrotalcite calcined)

ANALYSIS TECHNIQUES

Atomic Absorption Spectroscopy (AAS)

The elemental composition of the samples was determined by atomic absorption spectroscopy (AAS) using a Spectro-Analytical Instruments, Horiba Jobin–Yvon, Ultima spectrometer. An amount of the solid sample was dissolved in a mixture of HNO_3 and HF acids. The measurements were obtained by the method of addition of standard solution using Perkin-Elmer analyst equipment.

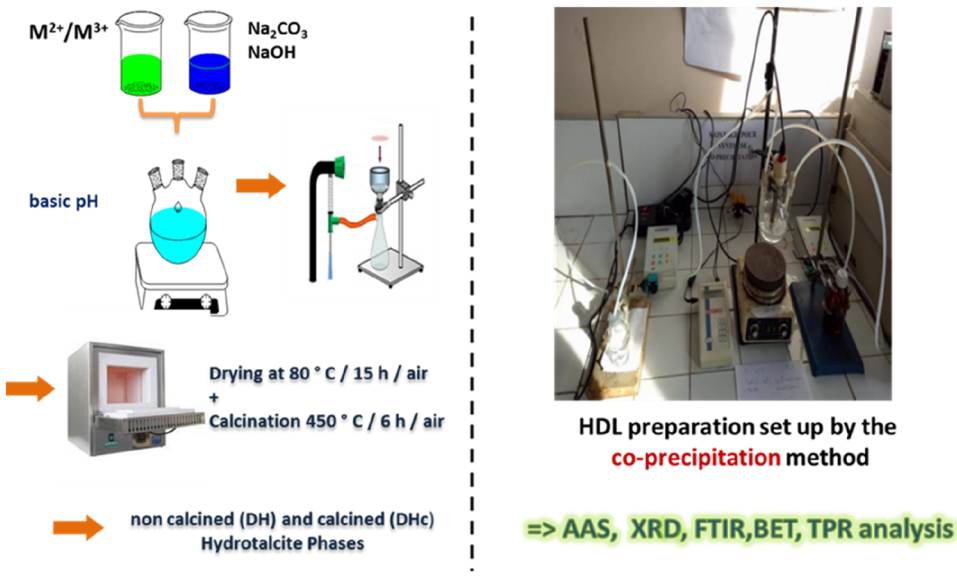

Fig. 4. Synthesis method and set-up description.

Brunauer–Emmett–Teller (BET) Analysis

The specific surface of the samples (BET surface) was measured with NOVA 2000e apparatus by adsorption of nitrogen at − 196°C by running some sorption/desorption cycles to investigate the nature of the pores from the adsorption isotherms. Before analysis, the samples underwent degassing under vacuum at 150°C for 2 h.

X-Ray Diffraction (XRD) Analysis

Powder x-ray diffraction (XRD) patterns were recorded with Siemens D-501 equipment using CuK_{α} *radiation* in the 2θ range between 10° and 80°. The crystallite size of the particle Ni^0 was evaluated using Scherrer's formula (Eq. 2).[4]

$$d_{hkl} = \frac{0.9\lambda}{\beta hkl \cos\theta} \quad (2)$$

where λ is the wavelength of CuKα (λ = 1.5418 Å), β_{hkl} is the half width of the peak, and θ is Bragg's diffraction angle. The dispersion ($D\%$) of the particle Ni^0 after reduction was estimated using the following equation[4]

$$D(\%) = \frac{971}{d_{\mathrm{Ni}\ (A)}} \quad (3)$$

Fourier Transform Infrared (FTIR) Analysis

FTIR spectra were recorded with a Perkin-Elmer spectrometer over 32 scans to improve the signal-to-noise ratio in the wavelength range (400–4000 cm^{-1}). The analysis was performed on ca. 4 mg of powder mixed with 100 mg of dried spectroscopic KBr pressed into pellets.

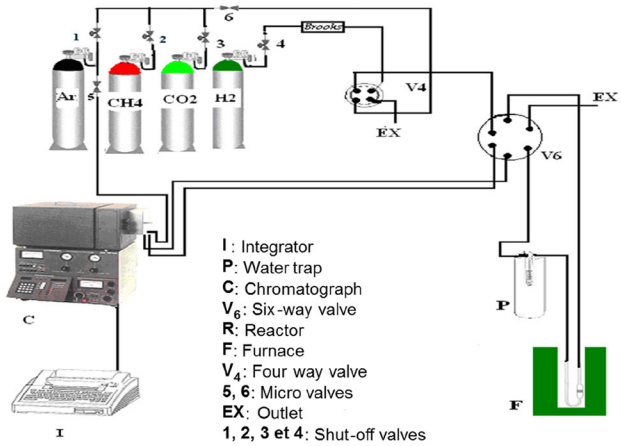

Fig. 5. Experimental set-up for the catalytic test.

Temperature Programmed Reduction (TPR)

Temperature programmed reduction (TPR) profiles were performed using a TriStar 3000 V6.01A apparatus equipped with a TCD detector. The reduction of samples was subsequently treated under 5% H_2/Ar with a flow rate of 50 mL/min from room temperature to 950°C with a heating rate of 10°C/min.

Catalytic Experiments

The catalytic activity tests were carried out at atmospheric pressure in a tubular quartz reactor by using the equipment presented in Fig. 5. Quartz wool was used as a support for the catalyst bed. For the reaction tests, typically 100 mg of catalyst was pre-treated under hydrogen at 650°C for 1 h. The reaction temperature, monitored by the thermocouple placed near the reactor wall, was increased from

room temperature to 650°C at the heating rate of 4°C/min. The reagent feed was controlled by mass flow controllers (Brooks 5850 TR). The reaction mixture CH_4: CO_2: Ar in volume proportion 20:20:60 at a flow rate of 20 ml/min was used for the reaction tests. This mixture could be passed through the sample by switching a four-way valve at the inlet of the reactor. The reagents and products were analysed in an on-line chromatograph (Delsi) equipped with a thermal conductivity detector (TCD) with a Carbosieve-B column using argon as the carrier gas.

After in situ reduction of the catalyst, the temperature of the furnace was maintained at the temperature of the reaction, and the hydrogen gas of the reduction was replaced by the reaction mixture (CH_4, CO_2) using the four-way valve (V4). The flow rate and composition of the reaction mixture were adjusted beforehand, and the reactants and products were sent through the six-way valve (V6) to the chromatograph for analysis. Before each catalytic test, "blank" tests were carried out under the same experimental conditions by "by-passing" the reactor.

RESULTS AND DISCUSSION

Catalyst Characterizations

The molar ratio of metal cations ($x = nM^{3+}/n(M^{2+} + M^{3+})$) in the synthesized catalysts was measured by atomic absorption spectroscopy and was equal to 0.30 and 0.31 for NiLa and NiMgLa, respectively (Table I). The values are similar to those obtained with hydrotalcite phases ($0.2 \leq x \leq 0.33$).[4] AAS analysis also showed the presence of minor anomalies in the molar ratio ($R = M^{2+}/M^{3+}$) compared to the theoretical report ($R = 2$). It is suggested that a small loss of metallic ions salt occurs during the precipitation and washing steps and accounts for the deficiencies in the total incorporation of the Ni into the brucite layers.

The BET measurements after calcination of NiLa and NiMgLa specimens are reported in Table I and adsorption isotherm curves are shown in Fig. 6. After calcination, the specific surface area decreases drastically for NiLa whereas it remains almost the same for NiMgLa. However, it should be mentioned that the BET area is twice as high in presence of Mg. This result is in agreement with those from Crivello et al.;[13] they reported that the incorporation of Mg in the hydrotalcite material leads to an increase in the specific surface. On the other hand, compared to our previous BET results for the catalysts NiMgAl-HT and NiAl-HT prepared by the same synthesis method presented in this work,[6] the NiMgLa-HD and NiLa-HL solids show lower specific surface values. The decrease in BET surface areas when La is added and replaced by Mg is probably due to the localization of La_2O_3 in the pores of the particles.

The nitrogen adsorption and desorption for the two calcined samples NiLa-DHc and NiMgLa-DHc are presented in Fig. 6. According to IUPAC classification,[14] nitrogen adsorption/desorption isotherms obtained for the two catalysts are of type IV with H1-type hysteresis loops for desorption isotherm typical to mesoporous solids.[15] This type of hysteresis is associated to the capillary condensation of compounds containing aggregates of platelet-like aggregates that are often obtained in the case of double lamellar and highlights a strong characteristic of mesoporous materials.[16] The hysteresis loop has parallel and nearly vertical adsorption and desorption branches. This type of hysteresis loop indicates that the solids have uniform pore sizes and meso-porosity of tubular shapes, open at both ends, whose section, circular or polygonal, varies little over the entire length of the tube.

The XRD analyses of uncalcined samples show a different structure from that of hydrotalcite (Fig. 7). Lamellar structures are absent and XRD patterns show the presence of low crystallinity. This result is attributed mainly to the large ionic radius of La^{3+} (116 pm) and to the amount of this element used to introduce it into the hydrotalcite matrix. It should be noted that all the trivalent ions that form the hydrotalcite structure have an ionic radius between 50 pm and 80 pm.[4] The presence of La in the hydrotalcite matrix causes a decrease in crystallinity. Lanthanum has a strong anionic radius, which promotes the formation of carbonate species in very early stages of co-precipitation and, in corroboration with its high anionic radius, prevented introduction and insertion of larger lanthanum elements into the HDL galleries.[4,9] Xie et al.[17] reported that the La cannot be incorporated into the HDL product layer network and replaced by Al^{3+} completely. This is probably due to the large difference in the ionic radius of the cations. Therefore, the optimal ratio of La^{3+} to Al^{3+} for the preparation of ZnAlLa-hydrotalcite is in the range

Table I. Molar ratios of metal cations, chemical composition and surface areas catalysts

Catalyst	$x = \frac{nM^{3+}}{n(M^{2+}+M^{3+})}$	$\frac{nM^{2+}}{nM^{3+}}$	Chemical composition	Ni/Mg ratio	Specific surface (m^2)/g Calcined
NiLa	0.30	2.30	$Ni_{0.69}La_{0.31}$	–	16
NiMgLa	0.31	2.19	$Ni_{0.14}Mg_{0.55}La_{0.31}$	0.25	31

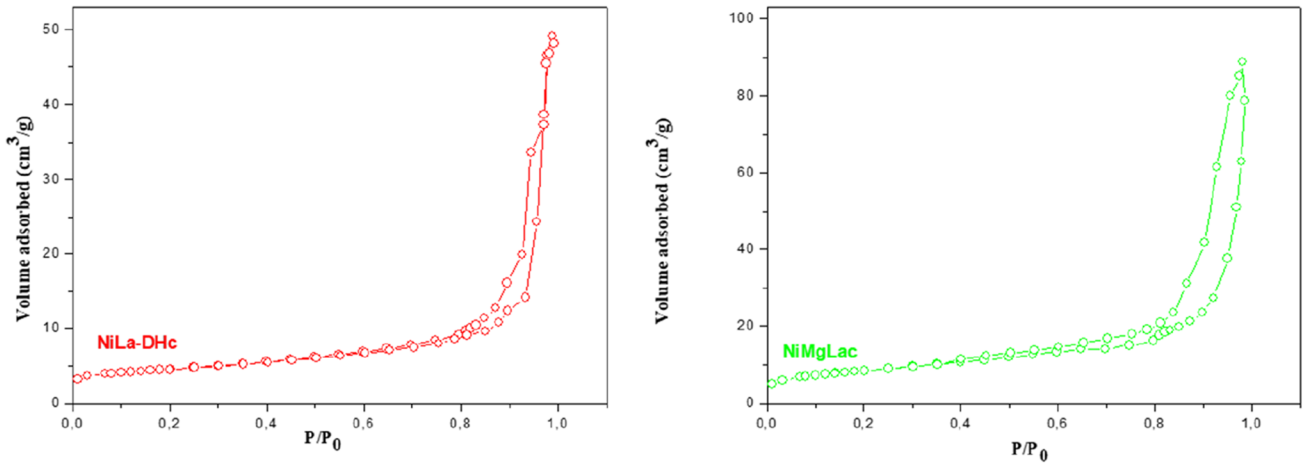

Fig. 6. Nitrogen adsorption/desorption isotherms of NiLa-DHc (left), NiMgLa-DHc (right).

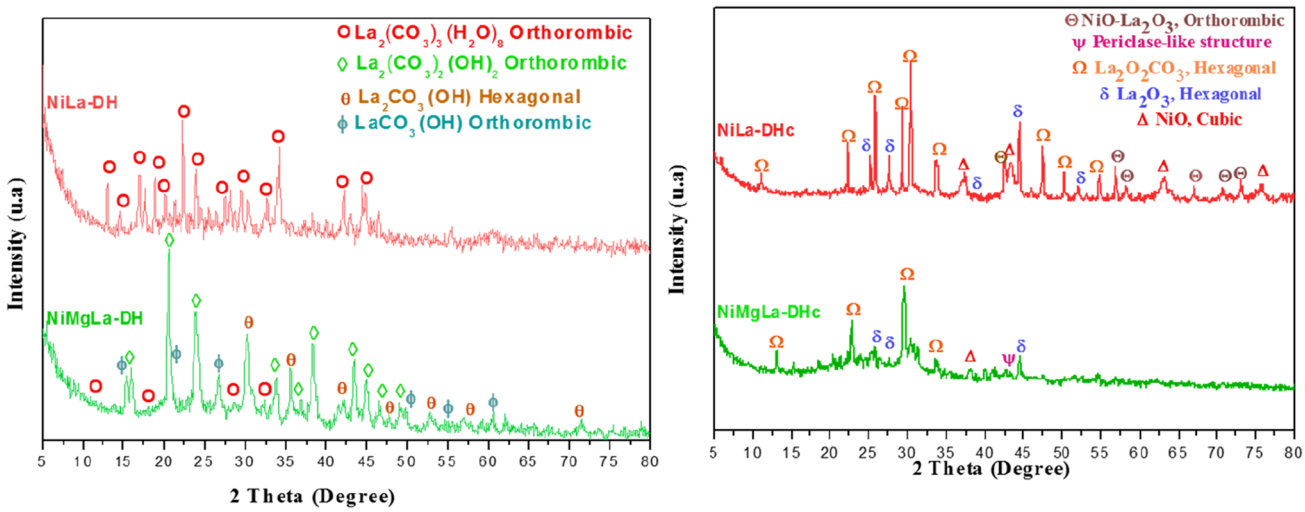

Fig. 7. X-ray diffractions of non-calcined (left) and calcined (right) samples.

of 0.07–2. In addition, the $La_2(CO_3)_2(OH)_2$ was observed in the case of both NiLa-DH and NiMgLa-DH samples.

The high ionic radius of lanthanum leads to the formation of lanthanum carbonate and oxyhydroxide phases at the beginning of coprecipitation, and its larger ionic radius prevented the insertion of La^{3+} into the hydrotalcite galleries.[9] After calcination, XRD patterns show the modification of the structure with presence of the new phases and the formation of oxides, and the periclase-like structure of mixed oxides occurs during calcination. In addition, the XRD analysis shows the presence of peaks corresponding to segregated phases of La_2O_3 and lanthanum oxycarbonate, which are probably formed by interaction with CO_2 from air.

FTIR analysis (Fig. 8) performed on uncalcined NiMgLa-DH and NiAl-DH samples reveals: (1) bands situated in the range 3000–3500 cm^{-1} are attributed to the stretching vibration of intercalated or adsorbed water molecules, (2) bands located at 1623 cm^{-1} are associated with the bending vibration of water presented in interlayer space and called water inter-lamellar, and (3) bands at 1380 cm^{-1} correspond to the asymmetric stretching mode of carbonate species in the interlayer spaces. Hydrotalcite type materials have a high affinity to absorb carbonates. (4) Bands identified at 1000 cm^{-1} are related to band translation mode between the metal and hydroxide group (M-OH), and (5) bands below 1000 cm^{-1} are attributed to the vibration mode of M–O–M′ (M = M(II), M′ = M(III)). After calcination, the intensity of all bands decreased because of the removal of physiosorbed and intercalated water molecules by dehydration and dihydroxylation with the removal of nitrate and carbonate molecules by decarbonation process (decarboxylation). These observations were confirmed by XRD analysis.

The H_2-TPR profiles obtained for the calcined solid samples NiLa-DHc-R and NiMgLa-DHc-R are presented in Fig. 9. The main reduction peaks detected in the TPR analysis correspond to the reduction of the nickel oxide phases. From a

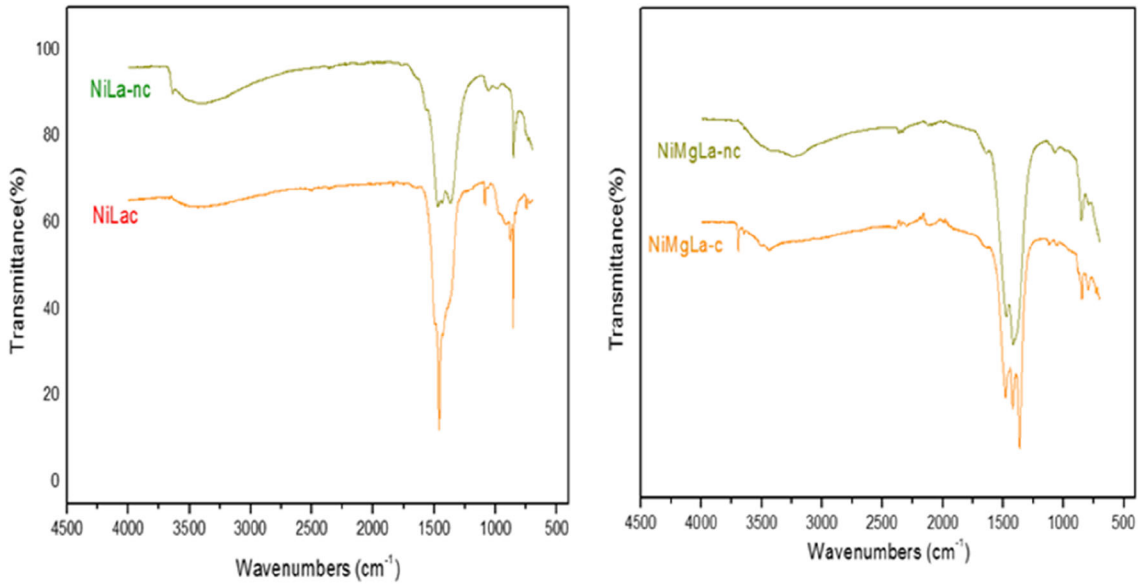

Fig. 8. FTIR spectrum of uncalcined and calcined NiLa (left) and NiMgLa (right) samples.

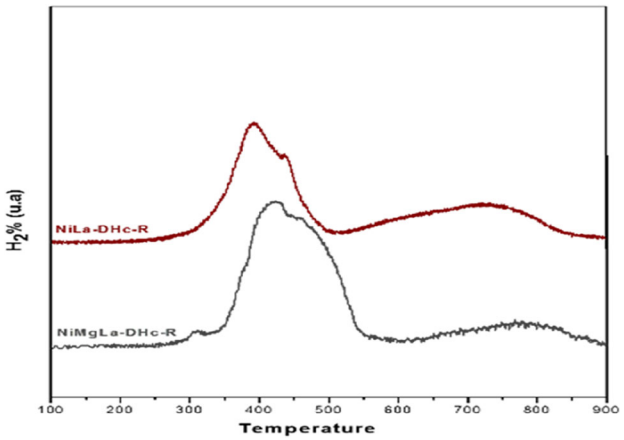

Fig. 9. TPR profiles measured NiLa-DHc-R and NiMgLa-DHc-R samples.

thermodynamic point of view, MgO and La_2O_3 cannot be reduced at these temperatures because of the low hydrogen partial pressure and high metal oxide stability. They were considered to have a stabilizing and supporting effect for Ni^{2+} cations.

From the TPR profile, a major peak centred around 400°C was observed and attributed to the reduction of free nickel oxides NiO. In addition, the same peak showing a shoulder at 500°C appeared for both NiLa-DHc-R and NiMgLa-DHc-R catalysts; a wider bump at about 750–800°C was also observed in both samples. For the NiLa-DHc-R catalyst, (1) the first and second peaks, centred at about 364°C and 409°C, were observed and could be attributed to surface NiO species, with either different size or different degree of interaction with the support, while the peak at higher reduction temperature, i.e., 722°C, corresponded to the reduction of mixed oxide phase such as $LaNiO_3LaNiO_4$ (La_2O_3–NiO).

The NiMgLa-DHc-R sample showed a minor first peak at 309°C, probably related to a small fraction of segregated NiO species, while peaks at about 426 and 468°C could be related to weakly bound NiO on the support surface. Finally, the fourth major peak at about 794°C was be attributed to the reduction of Ni incorporated into crystalline phases such as Mg (Ni, La)O periclase or perovskite-type $LaNiO_x$ phase.[18] The strong interaction between NiO and MgO resulted in a decrease in the reducibility of Ni due to the addition of La,[3] showing a higher reduction temperature compared to the NiLa-DHc-R sample. In the present work, the reduction temperature obtained with La-promoted samples was lower than that obtained with non-promoted solid hydrotalcite catalysts such as NiAl and NiMgAl.[6] Interestingly, the substitution of Al by La leads to a change in the reducibility of Ni species obtained from hydrotalcite-derived catalysts.[19] Furthermore, Yu et al.[20] found that the presence of lanthanum positively influences the reducibility of Ni particles by well-dispersed NiO species.

Catalytic Activity: DRM Catalytic Testing

The catalytic performances (conversion and selectivity) obtained with the two catalysts NiMgAl-DHc-R and NiLa-DHc-R in dry methane reforming are presented in Figs. 10 and 11. From these results, both samples are active in DRM reaction. An initial induction period is observed, which may be due to the interaction between CO_2 and La present on the catalysts.[10,11] However, the NiMgLa-DHc catalyst shows much better catalytic performances compared to NiLa-DHc-R. The conversion rates of CH_4 and CO_2 reach 99.3% and 99.4%, respectively, for the NiLa-DHc-R catalyst, while they reach 10.8%

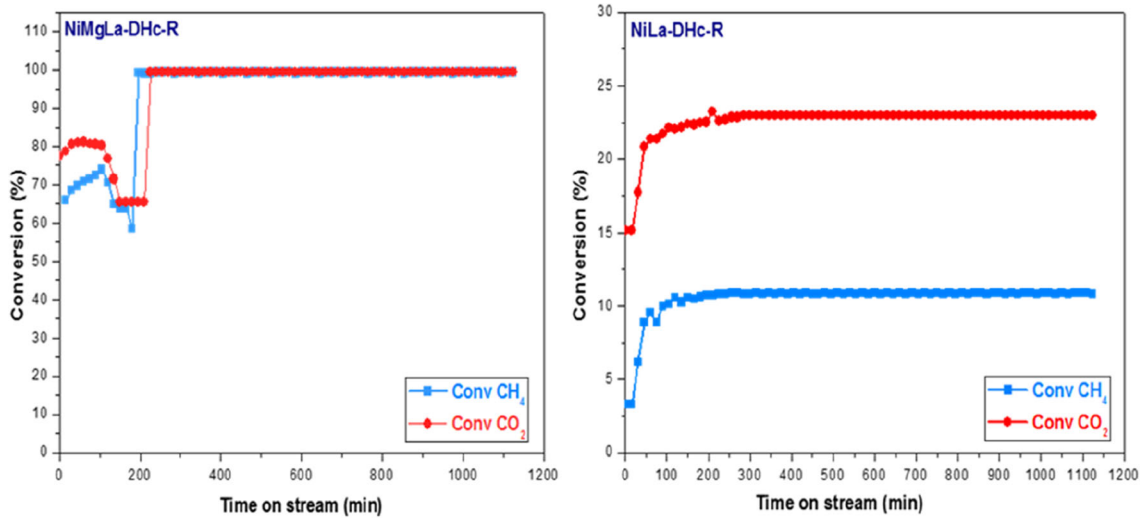

Fig. 10. Catalytic performances (conversion rate of CH_4 and CO_2) versus time at 650°C for NiLa-DHc-R and NiMgLa-DHc-R catalysts in dry reforming of methane ($T_{reaction}$ = 650°C, d_{MR} = 1.5 l/h, CO_2/CH_4 = 1.0)

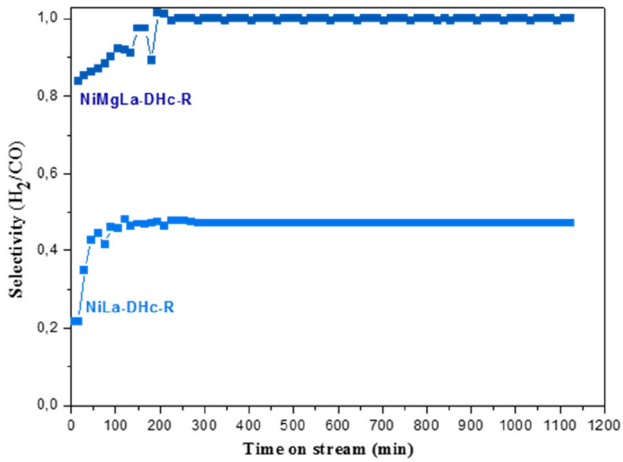

Fig. 11. Selectivity (H_2/CO) for the catalysts, NiLa-DHc-R NiMgLa-DHc-R versus time for NiLa-DHc-R and NiMgLa-DHc-R versus time at 650°C versus time ($T_{reaction}$ = 650°C, d_{MR} = 1.5 l/h, CO_2/CH_4 = 1.0)

and 22.9%, respectively, for NiLa-DHc-R. In addition, significant differences were also observed in the selectivity (represented by the H_2/CO_2 ratio, Fig. 11). NiMgLa-DHc-R shows almost equimolar conversion of CH_4 and CO_2, while it is close to 0.5 for the NiLa-DHc-R sample. The presence of H_2O as product (observed in the water trap) reveals side reactions, such as reverse water-to-gas shift reaction (RWGS), take place in NiLa-DHc-R but are almost absent in the case of NiMgLa-DHc-R. Wei et al.[21] attributed this phenomenon to a periodic cycle of carbon deposition and removal. Such a cycle with the catalyst may contribute to the stability of the catalytic performance.[22]

The obtained result reveals that the catalytic conversion on the lanthanum-promoted nickel-based catalysts exhibits a higher catalytic activity above the temperature of 650°C. Thus, the addition of lanthanum has a positive effect on the catalytic activity due to different factors:[9] (1) The presence of lanthanum favoured the formation of surface carbonates due to the promotion of basicity. (2) The formation of surface carbonates facilitated the rapid transport of CO_2 molecules to the interface between the metallic site and the support and thus accelerated the reaction of formation of intermediate CH_x species with CO_2. As a result, CH_x species and CO_2 were quickly converted to products. In addition, an increase in the surface Ni content of the catalysts improved reforming activity. (3) A slight improvement in the Ni metal dispersion could also be a minor factor in the improvement of catalytic activity.

For NiMgLa-DHc-R, the results show stoichiometric conversions of CO_2 and CH_4 should be the same for a CO_2/CH_4 ratio equal to 1 if the syngas is the only product. Both reactants apparently facilitate the dissociation of each other, as reported previously by Erdöhelyi et al.[23] However, the H_2 and CO products (or H_2/CO ratio) depend on the CH_4 and CO_2 conversions, the highest values obtained in the case of NiMgLa-HDL-R catalysts.

According to the literature,[6,7,24–27] the incorporation of Mg into the hydrotalcite matrix positively influences the catalytic performances and reactivity of the dry methane reforming. Indeed, the presence of Mg has many positive effects such as dispersive effect of Ni particles, acid–base properties and resistance to coke deposition as reported in the literature.[6,7,13,24] These results show that the combination of La with Mg can significantly improve the characteristics of the catalyst precursor for the DRM reaction. The crystal structure and

microstructural defects at high temperatures and low oxygen partial pressure seem to actively participate to the DRM reaction without poisoning the Ni particles. Currently, the reaction mechanism is not highlighted and needs further investigation to describe the correlation between the catalyst composition and its performance.

To summarize, NiMgLa-HDc-R shows higher catalytic performances compared to NiLa-HDc-R. This behaviour can be attributed to the role filled by the presence of Mg in combination with La, which leads to:

- Synergetic effect with the presence of lanthanum.
- Dispersive effect, with high specific surface especially after calcination.
- The formation of small fine particles with good dispersion.
- Stronger basicity properties.
- Adjusted acid-basic properties and compromise among reducibility, acid-basic characteristics and catalytic activity.
- Hgher Ni surface content.

These conclusions are similar to what has been observed in the literature.[13,28] However, the higher concentration of basic sites formed by samples with Ni/Mg ratio allows a better catalytic activity of the catalyst (synergetic effect).[7] In addition, according to our previous work,[28] the substitution of Al (acidic character) by La (basic character) allows obtaining more basic sites. In this case, a middle basic character can be favourable for dry reforming of methane under the catalytic conditions of our tests using lanthanum-nickel catalysts prepared from hydrotalcite. The same result was obtained by Yu et al.;[9] the lanthanum-containing catalysts showed high catalytic performance and the catalytic stability was significantly improved.

XRD Patterns After Reduction and DRM Catalytic Testing

The XRD patterns after reduction and catalytic dry methane reforming tests are presented in Fig. 12. For the reduced catalysts NiLa-DHc-R and NiMgLa-DHR, the phases presented have periclase structure and La_2O_3 segregated in addition to the presence of Ni particles phases at $2\theta = 44.7°$, 53° and 79°. However, the obtained results reveal that no carbon peaks were present for either NiLa-DHc-R or NiMgLa-DHc-R samples after the catalytic methane dry reforming test at 650°C. The presence of $La_2O_2CO_3$ took place by converting La_2O_3 with the absorption of CO_2 during the dry reforming of methane process. The phase $La_2O_2CO_3$ showed great behaviour by inhibiting a carbon deposition and eliminating coke around Ni active phase.[19] Therefore, it can be used to prevent the deactivation

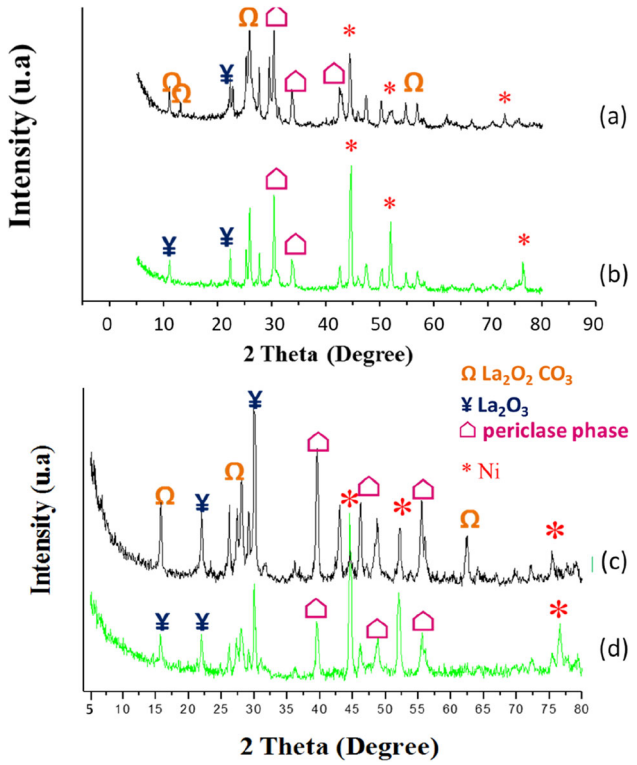

Fig. 12. XRD patterns of the reduced and spent La-promoted Ni-based catalyst derived from (a) NiLa-DHc-spent, (b) NiLa-DHc-R, (c) NiMgLa-DHc-spent, (d) NiMgLa-DHc-R catalysts

of the catalyst by cooking in different catalytic processes such as steam reforming of ethanol, dry reforming of methane and ethanol oxidative steam reforming.[19,29]

The crystallite sizes of Ni metal calculated from XRD patterns using Debye Scherrer equation with the dispersion ($D(\%)$) for NiLa and NiMgLa after reduction and catalytic methane dry reforming tests at 650°C are presented in Table II.

It should be noted that the Ni metal particle crystal size for the reduced catalyst NiMgLa-DHc-R was slightly smaller than that obtained by NiLa-DHc-R, indicating that the presence of lanthanum promoted the formation of small Ni particles especially in the case of NiMgLa-DHc-R. This result is additionally due to a synergetic effect with the presence of Mg, which has a dispersive character, leading to the formation of small, fine and well-dispersed particles as shown in Table II.

After catalytic testing of both samples in dry methane reforming at 650°C, a considerable reduction in crystal size takes place during the DRM reaction. The calculated particles size after the DRM tests is much smaller than that presented in the reduced catalysts (Table II). During the DRM process, the redistribution of Ni^0 particles takes

Table II. Particles sizes and dispersion of the reduced and spent catalysts

Catalysts	NiLa-HDc-R	NiMgLa-HDc-R	NiLa-HDc-spent	NiMgLa-DHc-spent
Particles sizes Ni (nm)	14	9	8	5
Dispersion (%)	7	11	13	21

place, probably due to the formation of isolated Ni species that are continuously extracted from the samples as reported by Liu et al.[19]

However, according to the characterization results obtained for both catalysts, they did not show any deactivation during the DRM reaction by sintering and/or carbon deposition. This is in good agreement with the results of DRM catalytic tests. The catalysts showed good catalytic activity and stability (Figs. 10, 11 and 12). In view of these results, the lanthanum-promoted nickel-based catalysts are considered promising for the dry reforming of methane at low temperature. The addition of lanthanum clearly improved the reactivity of dry reforming of methane at low temperature (650°C).

This work has opened up very interesting perspectives to be considered in the near future to study the lanthanum-promoted nickel-based catalyst in dry methane reforming; especially a detailed investigation of the mechanism is required to understand the catalytic behaviour of the low-temperature promoted nickel-based catalyst.

CONCLUSION

In this work, La-promoted Ni-based catalysts were prepared by coprecipitation at basic pH (pH = 11) for the DRM at low temperature of 650°C. However, the hydrotalcite structure was not obtained in the precursor state of the samples (probably because of the large ionic radius of La^{3+}) and/or the high content of La in the synthesis gel. Active and stable catalysts were prepared after calcination and reduction steps of these precursors. The two NiLa-DHc-R and NiMgLa-DHc-R catalysts did not show any deactivation during catalytic testing in the DRM reaction, which we attribute to a favourable promoter effect of La. The presence of lanthanum increases the absorption of CO_2 and improves the Ni content surface leading to improved catalytic performance and dry methane reforming stability and makes the catalysts more resistant to carbon deposition. The inhibition of the coke deposit on the surface of both catalysts (i.e., NiLa-DHc-R and NiMgLa-DHc-R) is due in particular to the presence of the $La_2O_2CO_3$ phase with good CO_2 absorption and dispersion of Ni metallic active phase particles. In addition, the NiMgLa-DHc-R sample shows much higher conversion and selectivity than NiLa-DHc-R sample, also highlighting the beneficial effect of Mg in combination with La.

ACKNOWLEDGEMENTS

The authors thank the General Directorate for Scientific Research and Technological Development (DGRSDT) of the Algerian Ministry of Higher Education for funding and technical support.

CONFLICT OF INTEREST

The authors declare that they have no conflict of interest.

REFERENCES

1. J.M. Lavoie, 2, 81 (2014). https://doi.org/10.3389/fchem.2014.0008.
2. X. Zhang, L. Zhang, H. Peng, X. You, C. Peng, X. Xu, W. Liu, X. Fang, Z. Wang, N. Zhang, and X. Wang, *Appl. Catal. B Environ*. 224, 488 (2018). https://doi.org/10.1016/j.apcatb.2017.11.001.
3. A. Serrano-Lotina, L. Rodríguez, G. Muñoz, A.J. Martin, M.A. Folgado, and L. Daza, 12, 961 (2011). https://doi.org/10.1016/j.catcom.2011.02.014.
4. F. Cavani, F. Trifirò, and A. Vaccari, *Catal. Today* 11, 173. https://doi.org/10.1016/0920-5861(91)80068-K (1991).
5. Z. Abdelsadek, M. Sehailia, D. Halliche, V.M. Gonzalez-Delacruz, J.P. Holgado, K. Bachari, A. Caballero, and O. Cherifi, 14, 98 (2016). https://doi.org/10.1016/j.jcou.2016.03.004.
6. Z. Abdelsadek, J.P. Holgado, D. Halliche, A. Caballero, O. Cherifi, S. Gonzalez-Cortes, and P.J. Masset, 151, 2696 (2021). https://doi.org/10.1007/s10562-020-03513-4.

7. Z. Abdelsadek, S. Gonzalez-Cortes, F. Bali, OuizaCherifi, D. Halliche, and P.J. Masset, 1 (2022). https://doi.org/10.1007/s11164-021-04640-2.
8. P. Li, F. Yu, N. Altaf, M. Zhu, J. Li, B. Da, and Q. Wang, *Materials*, 211, 1 (2018). https://doi.org/10.3390/ma11020221.
9. X. Yu, N. Wang, W. Chu, and M. Liu, *Chem. Eng. J.*, 209, 623 (2012). https://doi.org/10.1016/j.cej.2012.08.037.
10. X. E. Verykios, *Int. J. Hydrogen Energy*, 28, 1045 (2003). https://doi.org/10.1016/S0360-3199(02)00215-X.
11. A. Serrano-Lotina, L. Rodríguez, G. Muñoz, and L. Daza, *J. Power Sources*, 196, 4404 (2011). https://doi.org/10.1016/j.jpowsour.2010.10.107.
12. L. Shuirong, and G. Jinlong, *Chem. Soc. Rev.* 43, 7245. (2014).
13. M. Crivello, C. Pérez, J. Fernández, G. Eimer, E. Herrero, S. Casuscelli, and E. Rodríguez-Castellón, *Appl. Catal. A General*, 317, 11 (2007). https://doi.org/10.1016/j.apcata.2006.08.035.
14. G. Leofanti, M. Padovan, G. Tozzola, and B. Venturelli, *Catal. Today* 41, 207–219. (1998).
15. H.P. Bi, M. Guan, J.C. Li, and T.H. Liu, *J. Porous Mater*., 20 1299 (2013).
16. F. Rouquerol, J. Rouquerol, and K. Sing, Academic Press, London, (1999) 441.
17. X.I. Xie, X. An, X. Wang, and Z. Wang, 12, 259 (2003). https://doi.org/10.1016/S1002-0721(12)60151.
18. S.L. González-Cortés, I. Aray, and S.M.A. Rodulfor-Baechler, *J. Mater Sci.* 42, 6532. https://doi.org/10.1007/s10853-007-1552-7 (2007).
19. H. Liu, D. Wierzbicki, R. Debek, M. Motak, T. Grzybek, P. Da Costa, and M.E. Gálvez, 182, 8 (2016). https://doi.org/10.1016/j.fuel.2016.05.073.
20. X. Yu, N. Wang, W. Chu, and M. Liu, *Chem. Eng. J*., 209, 623 (2012). https://doi.org/10.1016/j.cej.2012.08.037.
21. J.M. Wei, B.Q. Xu, J.L. Li, Z.X. Cheng, and Q.M. Zhu, *Appl. Catal. A Gen*. 196, L167. https://doi.org/10.1016/S0926-860X(99)00504-9.
22. T. Richardson, principles of Catalyst Developement first ed., Plenum, New York, 1989, 167–172 (2000). https://doi.org/10.1002/adma.19910030320.
23. A. Erdöhelyi, J. Cserenyi, E. Papp, and F. Solymosi, *J. Catal*., 141, 287 (1993). https://doi.org/10.1006/jcat.1993.1136.
24. A. Djaidja, S. Libs, A. Kiennemann, and A. Barama, *Catal. Today*, 113, 194 (2006). https://doi.org/10.1016/j.cattod.2005.11.066.
25. K. Mette, S. Kühl, A. Tarasov, and T. Lunkenbien, *ACS Catal.*, 6 (2016) 7238.https://doi.org/10.1021/acscatal.6b01683..
26. J.Ã. Rivera, G. Fetter, Y. Jiménez, M.M Xochipa, and P. Bosch, *Appl. Catal. A General* 316, 207 (2007). https://doi.org/10.1016/j.apcata.2006.09.031.
27. Z. Abdelsadek, F. Touhra, K. Bachari, A. Saadi, O. Cherifi, and D. Halliche, Advanced Micro and Mesoporous Materials (Heron Press, Book Chapter), p. 60.
28. X. Zhang, L. Zhang, H. Peng, X. You, C. Peng, X. Xu, W. Liu, X. Fang, Z. Wang, N. Zhang, and X. Wang, *Appl. Catal. B Environ.*, 224, 488 (2018). https://doi.org/10.1016/j.apcatb.2017.11.001.
29. H.Q. Chen, H. Yu, F. Peng, and H.J. Wang, *J. Catal.*, 269, 281 (2010). https://doi.org/10.1016/j.jcat.2009.11.010.